A Hybrid Approach to Stress Analysis in Skeletal Systems

Alan Barhorst
Department of Mechanical Engineering
Texas Tech University
alan.barhorst@ttu.edu

Lawrence Schovanec
Department of Mathematics & Statistics
Texas Tech University
schov@math.ttu.edu

Abstract

This paper provides a continuum analysis of skeletal elastic structures in which loading conditions are derived from neural-musculotendon dynamics. Forward dynamic simulations of human motion are based on an ensemble of articulating segments controlled by Hill-type musculotendon actuators. The joint torques and reaction forces as predicted by this analysis determine loading conditions for the stress analysis of the segmental links which are modeled as hybrid parameter systems. This approach accounts for both the rigid body motions of the articulating links and the elastic deformations that represent the continuum effects in the bone. Although the methods in this paper are readily extended to general multi-link segmental models, simulations for the arm-shoulder complex are presented in order to illustrate the method.

1 Musculotendon Dynamics

Direct dynamic, or forward, models of human movement are utilized in this work in order to simulate human movement as a consequence of the applied muscle forces that are generated in response to a given neural stimulation. These muscle forces and joint passive effects determine the loading conditions that are incorporated into a stress analysis of elastic skeletal elements. The muscle models utilized in this investigation are referred to as a Hill-type models. They have been shown to incorporate realistic physiology and complexity while remaining computationally practical (see [2, 3] and references therein). In Figure 1, a phemenological model of muscle-tendon of length l_{tm} is depicted. The muscle of length l_m is in series and off-axis by a pennation angle α with the tendon of length l_t. The muscle is assumed to consist of two components: an active force generator and a parallel passive component. The passive component includes a parallel elastic element (F_{pe}) that describes the passive muscle elasticity and a linear damping component which corresponds to the passive muscle viscosity (B_m).

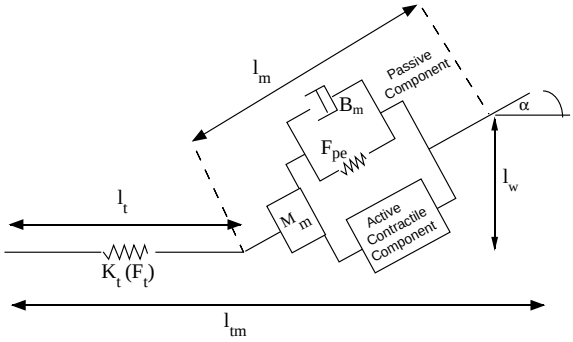

Figure 1. Hill Type Model of the musculotendon complex.

The model for the active contractile component is based on the generally accepted notion ([5]) that the active muscle force is the product of three factors: (1) a length-tension relation $f_l(l_m)$, (2) a velocity-tension relation $f_v(\dot{l}_m)$, and (3) the activation level $a(t)$. The length at which the maximum active muscle force, F_o, is developed is called the optimal muscle length, l_o. Consequently, it is convenient to visualize active force generation as a collections of surfaces obtained as a product of the nondimensionalized force velocity and force length curves scaled by activation,

$$F_{act} = a(t)F_o f_l(\tilde{l_m}) f_v(f_v(\dot{l}_m)).$$

where $\tilde{l}_m = l_m/l_o$. Several analytical models have been proposed to describe the curves $F_{pe},\ f_l(l_m)$ and $f_v(\dot{l}_m)$. The approach in this paper follows that previously employed in [2, 3] in which the active and passive force length curves and the force velocity curve are constructed from analytical models or as natural cubic splines fitted to physiological data.

Muscle activation, $a(t)$, is related to the neural input, $u(t)$, by a process known as contraction dynamics. The process through which neural input is transformed into activation is known to be mediated through a calcium diffusion process and is represented by the first order differential equation

$$\frac{da(t)}{dt} + \left[\frac{1}{\tau_{act}}\left(\beta + (1-\beta)u(t)\right)\right] a(t) = \frac{1}{\tau_{act}} u(t) \quad (1.1)$$

where $0 < \beta < 1$, $\beta = \tau_{act}/\tau_{deact}$, and τ_{act}, τ_{deact} are an activation and deactivation time constants that vary with fast and slow muscle.

The series elastic element in Figure 1 corresponds to the muscle tendon. More precisely, the tendon is assumed to behave non-linearly for small strains and then to become linear with stiffness constant k_s beyond a given level of force, F_{tc}. A common approach to tendon dynamics is to assume a model of the form [1]

$$\dot{F}_t = K_t(F_t)\dot{l}_t \tag{1.2}$$

where

$$K_t(F_t) = \begin{cases} k_{te}F_t + k_{tl} & 0 \le F_t < F_{tc} \\ k_s & F_t \ge F_{tc} \end{cases} .$$

From Figure 1 it readily follows that the total force of a muscle is the sum of the passive and the active forces, $F_m = F_{pe} + F_{act} + B_m\dot{l}_m$. The equation of motion for the muscle mass is expressed as

$$M_m \frac{d^2(l_m \cos\alpha)}{dt^2} = F_t - [F_{act}(a, l_m, \dot{l}_m) + F_{pe}(l_m) + B_m\dot{l}_m \cos\alpha. \tag{1.3}$$

Two state variables are required to describe the contraction dynamics of the musculotendon actuator as given by (1.2) and (1.3). A convenient choice that is least sensitive to the choice of initial conditions is $(F_t, \dot{l}_m)$. These states and $a(t)$ along with the differential equations (1.1),(1.2), and (1.3) describe the neural-musculotendon dynamics. These dynamics generate the active torques that are coupled to the kinematic dynamics of the hybrid mechanical system which are modeled using a hybrid mechanical approach.

2 Hybrid Parameter System

Modeling the articulated elastic segments coupled to the muscle dynamics described will be accomplished using a non-holonomic hybrid parameter projection method [4, **?**]. A set of field and boundary equations and the discrete coordinate ordinary differential equations are provided by the modeling method. These equations are minimal in the sense that the dynamics are projected on the constraint-free manifold of the generalized speed space and thus require no algebraic side conditions.

For purposes of illustration, the results presented here are for the case of the forearm. The system considered in this immediate work is shown in Figure 2.

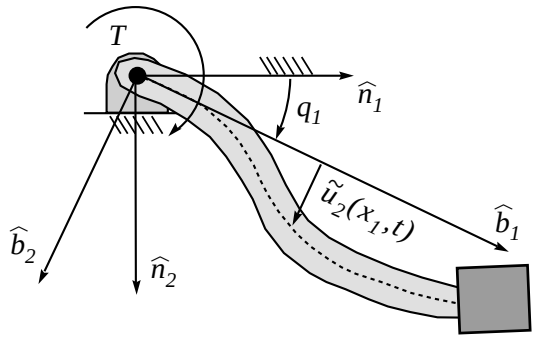

Figure 2. Single Link Arm With Load.

Shown in Figure 2 is the arm and load in a exaggerated deformed state so that coordinates can be clearly seen. The coordinate frame marked $\mathcal{N}$ is the Newtonian frame. Frame B rides with the undeformed state of the beam (body 1). The origin of both frames is o. The domain of the beam is one dimensional, the independent coordinate is x_1 measured from the root of the beam along the undeformed neutral axis of the beam. For this model we designate the loading torque shown as T. The coordinate measuring angular position of the beam is $q_1(t)$. The deflection of the beam is measured with $\tilde{u}_2(x_1, t)\hat{b}_2$ (simple flexure). The beam has mass per unit length ρ, its length is L, cross sectional area A, area moment of inertia I, and Young's modulus E. The tip mass is the second body. It is allowed both mass (M_w) and mass inertia (J_w) (relative to point b at the tip of the beam). Gravity g acts along the $\hat{n}_2$ direction.

The ordinary differential equation for angular rate $s_1 = \dot{q}_1$, can be formulated as [4],

$$0 = \frac{\partial {}^{\mathcal{N}}\vec{\omega}^{\,B_1}}{\partial s_1} \cdot \left[\vec{T}_1 - \vec{J}_1\right] + \frac{\partial {}^{\mathcal{N}}\vec{\omega}^{\,B_2}}{\partial s_1} \cdot \left[\vec{T}_2 - \vec{J}_2\right] + \frac{\partial {}^{o}\vec{v}^{\,b}}{\partial s_1} \cdot \left[\vec{F}_2 - \vec{I}_2\right] \tag{2.4}$$

where ${}^{\mathcal{N}}\vec{\omega}^{\,B_1}$ and ${}^{\mathcal{N}}\vec{\omega}^{\,B_2}$ are angular velocities for the arm and tip load, respectively and ${}^{o}\vec{v}^{\,b}$ is the tip velocity. The applied torques are $\vec{T}_1$ and $\vec{T}_2$. The inertia torques are $\vec{J}_1$ and $\vec{J}_2$. The tip mass inertia force is $\vec{I}_2$.

Assuming the forearm may be modeled as a Euler-Bernoulli beam, the strain energy density function for the link is given by

$$\bar{V} = \frac{1}{2}EI\left(\frac{\partial^2\tilde{u}_2}{\partial x_1^2}\right)^2. \tag{2.5}$$

The field equation for deflection can be derived ($i = 2$) from [4],

$$0 = \frac{\partial}{\partial x_1}\left(\frac{\partial \bar{V}}{\partial \tilde{u}_{2,1}}\right) - \frac{\partial^2}{\partial x_1^2}\left(\frac{\partial \bar{V}}{\partial \tilde{u}_{2,11}}\right) + \left(\vec{F}_B - \rho\, {}^{o}\vec{a}_{\mathcal{N}}^{\,dm}\right) \cdot \hat{b}_2, \tag{2.6}$$

where index notation is implied. The acceleration along the beam is given by ${}^o\vec{a}_{\mathcal{N}}^{dm}$ and body forces are $\vec{F}_B$. The boundary conditions ($i = 2$) are given by [4]

$$\frac{\partial \bar{V}}{\partial \widetilde{u}_{2,1}} - \frac{\partial}{\partial x_1}\left(\frac{\partial \bar{V}}{\partial \widetilde{u}_{2,11}}\right) = \frac{\partial^o \vec{v}^{\,b}}{\partial s_2'} \cdot \left[\vec{F}_2 - \vec{I}_2\right] \qquad (2.7)$$

$$\frac{\partial \bar{V}}{\partial \widetilde{u}_{2,11}} = \frac{\partial^{\mathcal{N}} \vec{\omega}^{\,B_2}}{\partial s_3'} \cdot \left[\vec{T}_2 - \vec{J}_2\right] \qquad (2.8)$$

for shear and bending, respectively, at $x_1 = L$. The pseudo-speeds [4] s_2', s_3' are defined as the rates of tip deflection and slope, respectively. At $x_1 = 0$ we have clamped conditions as seen form the rotating frame $\mathcal{B}$,

$$\widetilde{u}_2 = \widetilde{u}_{2,1} = 0 \qquad (2.9)$$

To integrate the equations of motion we formulate the partial differential equations in weak form with a two mode Hermite polynomial approximation to the displacement,

$$\widetilde{u}_2(x,t) = \left(\frac{3\,x_1^2}{L^2} - \frac{2\,x_1^3}{L^3}\right) q_2(t) + \left(-\frac{x_1^2}{L} + \frac{x_1^3}{L^2}\right) q_3(t). \qquad (2.10)$$

It then follows from equation 2.4 that,

$$\frac{g\,L^2\,\rho\,\cos(q_1(t))}{2} + T(t) - g\,M_w\,\sin(q_1(t))\,q_2(t) - \sin(q_1(t))\left(\frac{g\,L\,\rho\,q_2(t)}{2} - \frac{g\,L^2\,\rho\,q_3(t)}{12}\right) \cdot$$
$$2\,M_w\,q_2(t)\,s_1(t)\,s_2(t) - \frac{26\,L\,\rho\,q_2(t)\,s_1(t)\,s_2(t)}{35} + \frac{11\,L^2\,\rho\,q_3(t)\,s_1(t)\,s_2(t)}{105} + \frac{11\,L^2\,\rho\,q_2(t)\,s_1(t)\,s_3(t)}{105} - \frac{2\,L^3\,\rho\,q_3(t)\,s_1(t)\,s_3(t)}{105} + \left(-J_w - L^2\,M_w - \frac{L^3\,\rho}{3} - M_w\,q_2(t)^2 - \frac{13\,L\,\rho\,q_2(t)^2}{35} + \frac{11\,L^2\,\rho\,q_2(t)\,q_3(t)}{105} - \frac{L^3\,\rho\,q_3(t)^2}{105}\right)\dot{s}_1(t) + \left(-(L\,M_w) - \frac{7\,L^2\,\rho}{20}\right)\dot{s}_2(t) + \left(-J_w + \frac{L^3\,\rho}{20}\right)\dot{s}_3(t) = 0.$$

For the weak form of equations (2.6)-(2.9) associated to q_2 we have

$$g\,M_w\,\cos(q_1(t)) + \frac{g\,L\,\rho\,\cos(q_1(t))}{2} - \frac{12\,E\,I\,q_2(t)}{L^3} + \frac{6\,E\,I\,q_3(t)}{L^2} + M_w\,q_2(t)\,s_1(t)^2 + \frac{13\,L\,\rho\,q_2(t)\,s_1(t)^2}{35} - \frac{11\,L^2\,\rho\,q_3(t)\,s_1(t)^2}{210} - \frac{13\,\gamma\,L\,s_2(t)}{35} + \frac{11\,\gamma\,L^2\,s_3(t)}{210} + \left(-(L\,M_w) - \frac{7\,L^2\,\rho}{20}\right)\dot{s}_1(t) + \left(-M_w - \frac{13\,L\,\rho}{35}\right)\dot{s}_2(t) + \frac{11\,L^2\,\rho\,\dot{s}_3(t)}{210} = 0$$

A proportional viscous damping body force was assumed present with damping constant γ. The weak form of equations (2.6)-(2.9) associated with q_3 is expressed as

$$\frac{-\left(g\,L^2\,\rho\,\cos(q_1(t))\right)}{12} + \frac{6\,E\,I\,q_2(t)}{L^2} - \frac{4\,E\,I\,q_3(t)}{L} - \frac{11\,L^2\,\rho\,q_2(t)\,s_1(t)^2}{210} + \frac{L^3\,\rho\,q_3(t)\,s_1(t)^2}{105} + \frac{11\,\gamma\,L^2\,s_2(t)}{210} - \frac{\gamma\,L^3\,s_3(t)}{105} + \left(-J_w + \frac{L^3\,\rho}{20}\right)\dot{s}_1(t) + \frac{11\,L^2\,\rho\,\dot{s}_2(t)}{210} + \left(-J_w - \frac{L^3\,\rho}{105}\right)\dot{s}_3(t) = 0$$

The three kinematic differential equations are:

$$\dot{q_1}(t) - s_1(t) = 0 \qquad (2.11)$$
$$\dot{q_2}(t) - s_2(t) = 0 \qquad (2.12)$$
$$\dot{q_3}(t) - s_3(t) = 0 \qquad (2.13)$$

where $q_1 = \theta$, q_2 denotes the tip deflection, q_3 the tip rotation.

The above kinematic differential equations of motion are coupled to the control equations via the torques $T(t)$. These torques reflect the combined moment due to the muscle forces and the joint passive effects. The joint effects result in passive moments that can be modeled as in [3] and take the form

$$M_p(\theta, \dot{\theta}) = k_1 e^{-k_2(\theta - \theta_{min})} - k_3 e^{-k_4(\theta_{max} - \theta)} - c\dot{\theta} \qquad (2.14)$$

where θ denotes the limb angle and $\theta_{min} \leq \theta \leq \theta_{max}$ where k_1, k_2, k_3, k_4, and c are shape parameters. The moment arms through which the tendon forces produce active torque were modeled by polynomials fitted to data in Pigeon *et. al.* ([6]).

The limb and contraction dynamics can now be represented in terms of states that correspond to the kinematic variables, $q_1, q_2, q_3, s_1, s_2, s_3$ which are coupled via the torques $T(t)$ to the neural-musculotendon variables, $F_t, \dot{l}_m, a(t)$.

3 Numerical Simulations and Conclusions

Numerical illustrations for ballistic and active simulations are presented. In the first case, the forearm is released at rest from the horizontal position with a load of 10kg. Figures 3 and 4 show the joint angle q_1 and the tip displacement as a $\widetilde{u}_2(l,t)\hat{b}_2$, where l is the length of the link (see Figure 2).

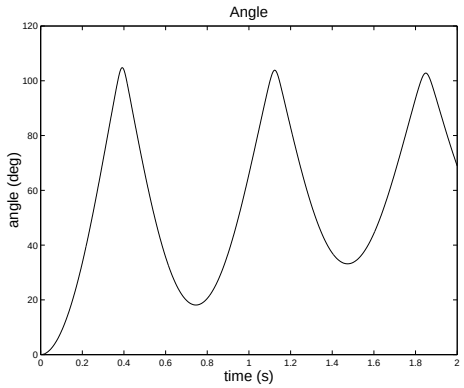

Figure 3. Limb joint displacements-ballistic.

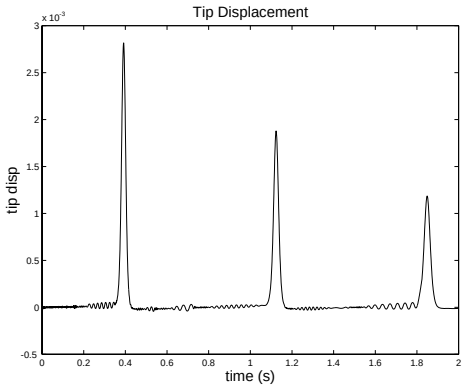

Figure 4. Tip displacements-ballistic.

As expected the arm settles into an equilibrium position corresponding to hanging straight down and the only measurable tip deflections occur when the motion is impeded by the soft constraints due to the passive joint effects in equation (2.14).

In Figures 5, 6, and 7, results are presented when the arm starts from the vertical position and a neural stimulus is provided that activates the agonist muscle. In this case $u(t)$ in equation (1.1) was modeled as a step input of maximal stimulation and a duration .25 seconds. One observes that strains of less than 1% are computed, which, as expected, are several orders of magnitude less than the tendon strains.

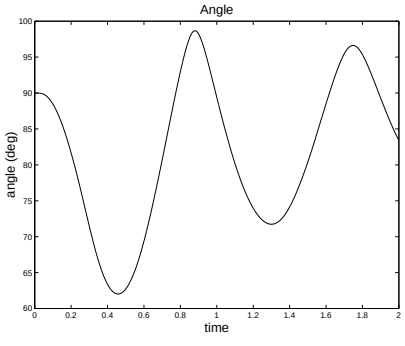

Figure 5. Limb joint displacements-active.

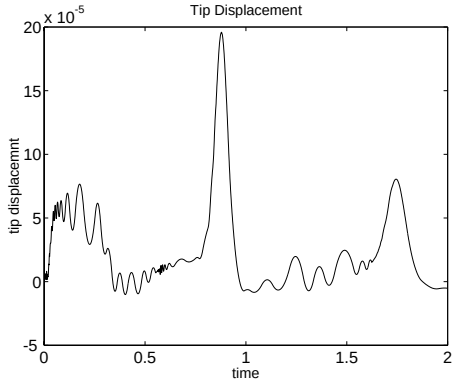

Figure 6. Tip displacements-active.

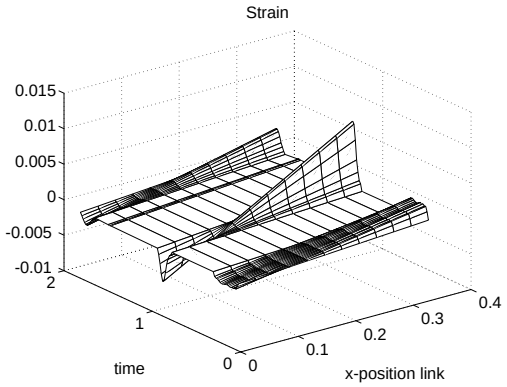

Figure 7. Strains along the length of the link.

In summary, this work provides a connection between neurological controls and the strain and stress that develops in bone. The continuum analysis that is carried out not only incorporates dynamic effects due to muscular loading, but allows for very general constitutive properties that are relevant to the accurate description of bone and connective tissue. Such an approach provides the capability to examine several issues that are of importance in analyzing failure in the skeletal system. For example, by the methods presented here, it is possible to examine the connection between neural and muscular activity and stress fractures and the manner in which strain energy is distributed between musculotendon actuators and skeletal segments.

References

[1] He, J. , Levine, W. Feedback Gains for Correcting Small Perturbations to Standing Posture. *IEEE Transactions on Automatic Control*, vol 36, 322-332, 1991.

[2] Schovanec, L., Martin, C.F. The Control and Mechanics of Human Movement System, *Dynamical Systems, Control, Coding, Computer Vision: New Trends, Interfaces, and Interplay* (G. Picci, D. Gilliam, Eds.), Birkhauser, 173-202, 1999.

[3] Dewoody, Y. , Schovanec, L. A Forward Dynamic Model of Gait with Application to Stress Analysis of Bone, Accepted for publication in *J. of Mathematical and Computer Modeling*.

[4] Barhorst, A. and Everett, L. Modeling hybrid parameter multibody systems, *Int. J. Nonlinear Mechanics*, **30**:1-21, 1995.

[5] Zajac, F.E. Muscle and tendon: Properties, models, scaling, and application to biomechanics and motor control. *In CRC Critical Reviews in Biomechanical Engineering.* **17**: 359-410 (1989).

[6] Pigeon,P, . Yahia, L. and Feldman, A.. Moment arms and lengths of human upper limb muscles as functions of joint angles. *J. Biomechanics*, 29(10): 1365-1370, 1996.